A SPATIAL VARIABILITY VIEW OF FREEWAY-3 DIP SLOPE FAILURE IN TAIWAN

Jianye Ching [1] and Hung-Jiun Liao [2]

ABSTRACT

During the investigation of a Freeway-3 (F-3) dip slope failure in Taiwan, it was found that the uncertainty involved in the spatial variability of material strength and groundwater condition had a significant influence on the stability analysis of the slope. This study aims to conduct a forensic analysis for the Freeway-3 case from the perspective of spatial variability of shear strength in the slope. Analysis results show that under the information available at the design stage (around 1995), the original design of the Freeway-3 dip slope has a fairly acceptable risk level if spatial variability is not considered. If spatial variability is properly considered, the risk level dramatically worsens. Together with the new evidence obtained in the 2010 forensic investigation, the risk level worsens to "hazardous". Spatial variability seems to be able to explain why there was a sudden increase in anchor loads during the construction stage in December 1997. In the premise that the critical weak layer has been identified, simple risk-based design steps are proposed in this study. These steps do not require detailed spatial variability analysis because the analytical equations regarding spatial variability has been calibrated in this study.

Key words: Dip slope failure, Freeway-3 case, spatial variability, failure probability, risk.

1. INTRODUCTION

On April 25 2010, a large scale dip slope failure occurred at chainage 3.1K of Freeway-3 (F-3) in Taiwan with four fatalities. Slope mass slid down along a 4-5 m thick soft shale layer underlying the slope. This shale layer will be referred as the "critical layer" later. It is widely accepted that this dip slope failure was caused partly by the corrosion of the ground anchors and partly by the groundwater induced degradation of the shear strength in the critical layer (TGS 2011).

Long before 2010, the sign of the failure first occurred in December of 1997, when the slope toe was cut further to 5.5 m below the freeway surface for the launching pit of incremental bridge construction. The anchor loads suddenly increased from around 70 tons to 76 ~ 87 tons (design load = 60 tons) and were later temporarily stabilized after the backfill of the 5.5 m cut. This sudden increase in the anchor loads during the launching pit construction cannot be explained as the consequence of the anchor corrosion and sliding surface degradation, as both mechanisms require a long period of time. This sudden increase was rather unexpected, as the design of the anchored slope was expected to be fairly safe. A weak critical layer was identified in the design stage in 1995. The site investigation revealed that the nominal cohesion and nominal friction angle of the critical layer were about 9.8 kN/m^2 and 20°, respectively at the design stage. Even the cohesion is assumed to be zero, the nominal friction angle 20° is significantly larger than the dip angle of 14° ~ 15° for the potential sliding surface. In fact, the design factors of safety (FS) of two typical sections were satisfactory: FS > 1.5 for normal condition, FS > 1.1 with design earthquake, and FS > 1.2 with design rainfall. The cause of this sudden increase in the anchor loads is not yet clear following the parameters used for design.

A possible yet rarely explored explanation for the dip slope failure and the sudden increase in the anchor loads is the spatial variability of the shear strength in the critical layer. The spatial variability of the shear strengths in the critical layer of thickness T can be illustrated with Fig. 1. The critical shale layer is not homogeneous, and its properties are expected to vary in space. In the upper plot of Fig. 1, the direction perpendicular to the bedding plane is denoted by the N-direction, while the dip direction of bedding plane is the D-direction. Due to the natural deposition process, the shear strength of the critical layer is expected to vary drastically in the N-direction but mildly in the D-direction. A schematic of the spatial variability of shear strength [in term of tan (ϕ)] in the N-direction is illustrated in the lower plot of Fig. 1.

Site investigation cannot explore the full profile of the shear strength but only a few sampled values. The crux of the spatial variability is that the overall shear strength is governed by the minimum value in the shear strength profile (see the lower plot in Fig. 1). This minimum value is very likely to be less than the sampled (nominal) value. In practice, the nominal shear strength is divided by the factor of safety (typically 1.5 for slopes) to obtain the design value. What if the sampled value is unfortunately on the high side of the shear strength profile? Can we design based on the (simulated) minimum value?

The difference between the nominal value and the minimum value depends on two factors: (a) the amplitude of fluctuation and (b) the scale of fluctuation (SOF) (see the lower plot in Fig. 1). The amplitude of fluctuation governs the amplitude of the fluctuation from the mean value, while the SOF governs the number of fluctuation cycles within the entire thickness T. When SOF is small so that T/SOF is large (many fluctuation cycles), the minimum value in the shear strength profile may be substantially smaller than the nominal value, and vice versa.

Manuscript received December 14, 2012; revised March 15, 2013; accepted March 19, 2013.

[1] Professor (corresponding author), Dept of Civil Engineering, National Taiwan University, Taipei, Taiwan (e-mail: jyching@gmail.com).

[2] Professor, Dept of Construction Engineering, National Taiwan University of Science and Technology, Taipei, Taiwan.

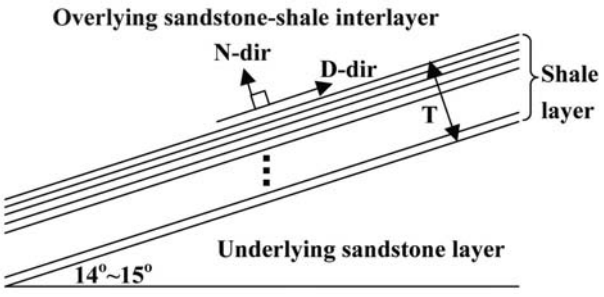

(a)

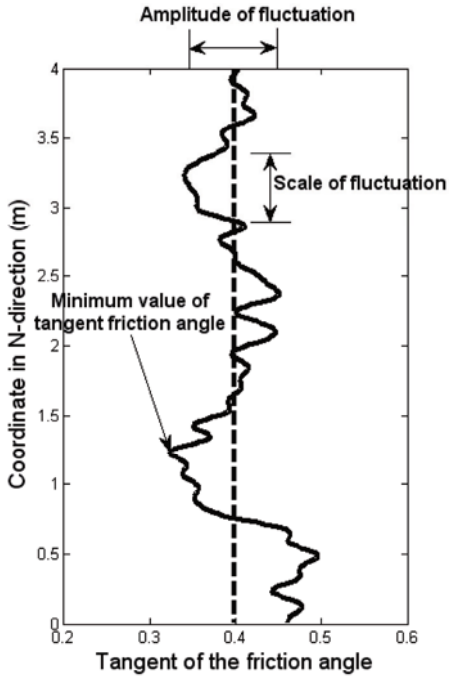

(b)

Fig. 1 (a) Schematic for the critical shale layer of thickness *T*; (b) schematic for the *N*-direction spatial variability of tangent friction angle in the critical layer

The key question is: How to model the aforementioned difference between the nominal value and the minimum value? Can such a spatial variability model explain the sudden increase in the anchor loads during the launching pit excavation stage and also the dip slope failure of the Freeway-3 case? The main purpose of this study is to address these questions. In this paper, spatial variability of tan (ϕ) in the critical layer will be studied, where ϕ is the residual friction angle of the critical layer. The residual cohesion (c) will be ignored because it is not reliable. The shorthand notation t_f will be used to denote tan (ϕ). Only the spatial variability of t_f in the *N*-direction of the critical layer will be considered, as the spatial variability in the *D*-direction is expected to be far less significant. The notation $t_f(z)$ is used to denote tan[$\phi(z)$] at a location of $z \in [0, T]$, where z is the coordinate for the *N*-direction and $T = 4$ m.

It is worth mentioning that the identification of the critical layer itself is a challenging task that cannot be easily achieved even with a detailed site investigation. The location of the actual slip surface for the Freeway-3 case was uncertain until the failure occurred. As a result, the shale layer is known to be critical only after the failure event. The purpose of this study is not to address how to identify such a critical layer beforehand. Rather, its purpose is to conduct a forensic analysis about the impact of spatial variability in the critical layer and to provide plausible explanation to some observed phenomena, given that the critical layer has been identified.

The approach taken in the current paper is somewhat different from that taken in Wang *et al*. (2013). In Wang *et al*. (2013), an inverse Bayesian analysis is conducted to identify the posterior distribution of the friction angle in the critical layer, given the information that the Freeway-3 case has failed. They concluded that the friction angle is with posterior mean = 13.0° ~ 13.2° and posterior standard deviation = 1.0° ~ 1.5°. However, the current study shows that if spatial variability is properly considered, even the forward analysis (the information that the Freeway-3 case has failed is not used) indicates that the Freeway-3 case had unacceptably large risk.

2. SPATIAL VARIABILITY OF GEOTECHNICAL MATERIALS

Spatial variabilities of soil and rock properties are usually modeled by random fields (Vanmarcke 1977). Among random field models, stationary random fields are widely used due to their simplicity and possibly the only practical version that can be characterized from limited data (Phoon *et al*. 2003). A one dimensional stationary random field for shear strength $t_f(z)$ can be characterized by its mean value μ, coefficient of variation [COV = (standard deviation)/(mean value)], and correlation function. The correlation function of a stationary random field $t_f(z)$ is used to model the correlation between two locations with Δz apart in the *N*-direction:

$$\rho(\Delta z) = \rho\left[t_f(z),\ t_f(z+\Delta z)\right] = \frac{CV\left[t_f(z),\ t_f(z+\Delta z)\right]}{\sqrt{Var\left[t_f(z)\right]}\cdot\sqrt{Var\left[t_f(z+\Delta z)\right]}} \quad (1)$$

where $Var(.)$ denotes variance; $CV(.,.)$ denotes covariance. The hypothesis of stationarity allows ρ to be function Δz only, rather than the absolute coordinates z and $z + \Delta z$ (see left hand side of Eq. (1). The most popular correlation model in geotechnical engineering is the single exponential model (Vanmarcke 1977):

$$\rho(\Delta z) = \exp(-2\,|\,\Delta z\,|\,/\,\delta_z) \quad (2)$$

where δ_z is the scale of fluctuation (SOF) in the *N*-direction. It is clear that the correlation decreases as Δz increase. This is commonly observed in natural soils and rocks: Soil and rock properties are strongly correlated within a small interval and are weakly correlated when located far apart. When δ_z approaches infinity, $t_f(z)$ becomes a constant function, *i.e.*, homogeneity.

The spatial variability of $t_f(z)$ can be simulated by Fourier series expansion (Jha and Ching 2013). Figure 2 shows simulated $t_f(z)$ profiles in an interval of 4 m with mean value μ = 0.4, COV = 0.2, and δ_z = 1 m, 10 m, and 100 m. It is clear that the effect of δ_z is to change the number of fluctuation cycles – the smaller δ_z, the more cycles. The dip slope will fail when the minimum value of tan [$\phi(z)$] within $z \in [0, T]$ is less than the limiting value $t_{f,L}$, *i.e.*, $\min_{z\in[0,T]} t_f(z) < t_{f,L}$.

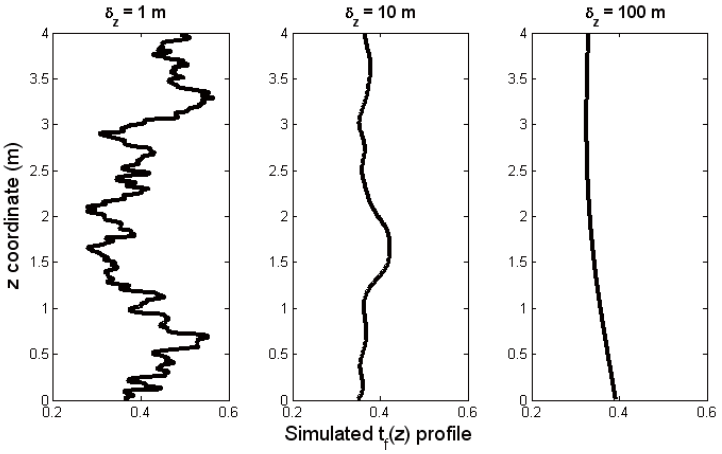

Fig. 2 Simulated $t_f(z)$ profiles for various δ_z

3. ESTIMATION FOR μ, COV, AND δ_Z FOR CRITICAL LAYER

Table 1 lists the shear strength test results (residual strength) for two rock samples obtained from the critical layer (the ⑤SH layer in Fig. 3). This layer was identified to be the layer that contains the actual failure surface (TGS 2011). The average thickness (T) of the critical layer is 4 m. The two samples were obtained from boreholes at the downhill side of this dip slope formation (see Fig. 3). They were not obtained directly from the uphill original slope that failed during the Freeway-3 event: This slope has slid away during the event and was then removed afterward. Both samples were tested under not submerged condition.

It is not trivial to determine μ, COV, and δ_z for the $t_f(z)$ in the critical layer from limited test results in Table 1. Based on the two samples, the best estimate for μ is (0.418 + 0.251)/2 = 0.335. However, these two samples are insufficient to determine COV and δ_z. Table 2 summarizes a database of the residual friction angles of the sandstone-shale interlayers (SS/SH) and shale (SH) in northern Taiwan. Although the mean value μ varies widely among various locations, the COV is fairly uniform and is around 0.2 for five locations. This COV of 0.2 is consistent to the average COV of the spatial variability in clay's tan(ϕ) summarized by Phoon (1995) based on a database of four sites [Table 4-1 in Phoon (1995) suggests that such COV is on average 0.2 ~ 0.23]. This consistency is deemed reasonable – shale is formed from clays, and it is fairly reasonable to see their COVs are close. As a result, COV = 0.2 seems to be a reasonable estimate for the critical layer in the Freeway-3 case.

Given that COV of t_f = 0.2 is reasonable, the likelihood of obtaining the two data points in Table 1 can be expressed as follows (assume Gaussian distribution):

$$\mathrm{L(data)} = \frac{1}{2\pi}\frac{1}{\sqrt{|\Sigma|}}\exp\left(-0.5\begin{bmatrix}0.418-\mu\\0.251-\mu\end{bmatrix}^T\Sigma^{-1}\begin{bmatrix}0.418-\mu\\0.251-\mu\end{bmatrix}\right)$$

$$\Sigma = (0.2\mu)^2\begin{bmatrix}1 & \exp(-2\Delta z/\delta_z)\\ \exp(-2\Delta z/\delta_z) & 1\end{bmatrix}$$

$$\approx (0.2\mu)^2\begin{bmatrix}1 & \exp(-1.5/\delta_z)\\ \exp(-1.5/\delta_z) & 1\end{bmatrix} \quad (3)$$

where L(data) is the likelihood of the dataset; 0.2μ is the standard deviation of t_f; Σ is the covariance matrix of the two data points; $\Delta z \approx 0.75$ m is the distance between the two samples in the N-direction. For a Gaussian distribution with COV = 0.2, the chance of getting a negative value of t_f is less than 3.0E–7. As a result, the Gaussian assumption will not bring much trouble in the aspect of absurd negative t_f values. Consider two scenarios:

1. Scenario D (design stage): The value of μ = 0.4 is chosen – this corresponds to ϕ = 21.8°, close to ϕ = 20° that was chosen during the design stage of the Freeway-3 dip slope in 1995. The minor difference of 1.8° may accommodate the ignored residual cohesion of c = 9.8 kN/m^2.
2. Scenario F (forensic investigation): The value of μ = 0.335 is chosen – this is based on the average value of t_f = tan (ϕ) for the two data points obtained during the forensic investigation in 2010 (Table 1).

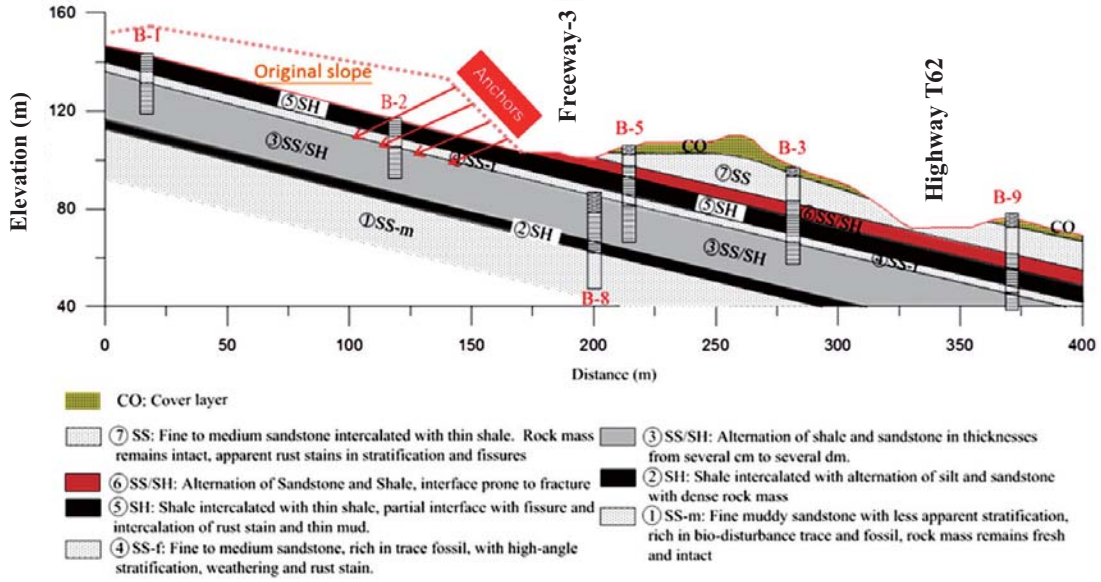

Fig. 3 A cross section of the Freeway-3 event site [modified from Fig. 5 ~ 14 in TGS (2011)]

Table 1 Shear strength test results for two rock samples obtained from the critical layer [extracted from Table 5 ~ 7 in TGS (2011)]

Specimen index	Borehole	z (m)	Residual strength		$t_f = \tan(\phi)$
			c (kN/m^2)	ϕ (degree)	
RDS(D)-5	B-7	0.75 m*	0.0	22.7	0.418
RDS(W)-4	B-5	1.5 m*	0.0	14.1	0.251

* Estimated z coordinates

Table 2 Database of residual (c, ϕ) for northern Taiwan [based on the database in Ching *et al.* (2012)]

Location	Residual strength		$t_f = \tan(\phi)$	μ of t_f	COV of t_f	Rock type
	c (kN/m^2)	ϕ (degree)				
Muzha Dist. (Taipei City)	0	43.4	0.946	0.749	0.231	SS/SH*
	0	34.3	0.682			
	0	31.8	0.620			
Shenkeng Dist. (New Taipei City)	0	32.9	0.647	0.658	0.185	SS/SH
	0	32.7	0.642			
	0	27.6	0.523			
	0	39.3	0.818			
Rueifang Dist. (New Taipei City)	0	21	0.384	0.345	0.175	SS/SH
	0	23	0.424			
	0	17	0.306			
	0	17	0.306			
	0	21	0.384			
	0	15	0.268			
Xindian Dist. (New Taipei City)	0	30	0.577	0.518	0.237	SS/SH
	0	24.6	0.458			
	0	23.5	0.435			
	0	28	0.532			
	0	19	0.344			
	0	26	0.488			
	0	28.6	0.545			
	0	37.3	0.762			
Xinyi Dist. (Taipei City)	0	19.5	0.354	0.377	0.067	SS/SH
	0	22	0.404			
	0	20.5	0.374			
Xindian Dist. (New Taipei City)	0	26.5	0.499	0.508	0.187	SH*
	0	23.5	0.435			
	0	21.8	0.400			
	0	30.2	0.582			
	0	32	0.625			

* SS/SH denotes sandstone-shale interlayer; SH denotes shale

In summary, scenario D is consistent to the information status adopted during the design stage in 1995, and scenario F is consistent to the information status during the forensic investigation in 2010.

Figure 4 shows the likelihoods versus δ_z for the two scenarios. For scenario D and F, the likelihood L(data) is maximized when δ_z = 7.0 m and 5.5 m, respectively. These estimates for δ_z agree well with the range of the vertical scale of fluctuation for shear strengths of clays [Table 4-4 in Phoon (1995) suggests that such δ_z is between 0.8 m ~ 6.1 m and is on average 2.5 m]. Again, this consistency is deemed reasonable, as shale is formed from clays, and it is reasonable to see their SOF's are close. Table 3 summarizes the best estimates for μ, COV, and δ_z for the t_f in the critical layer under the two scenarios.

Table 3 Best estimates for μ, COV , and δ_z for the t_f in the critical layer for the two scenarios

Scenario	μ of t_f	COV of t_f	δ_z (m)	Remark
D	0.4	0.2	7.0	Consistent to the information status during the design stage (c = 9.8 kN/m^2, ϕ = 20^o)
F	0.335		5.5	Consistent to the information status during the forensic investigation (Table 1)

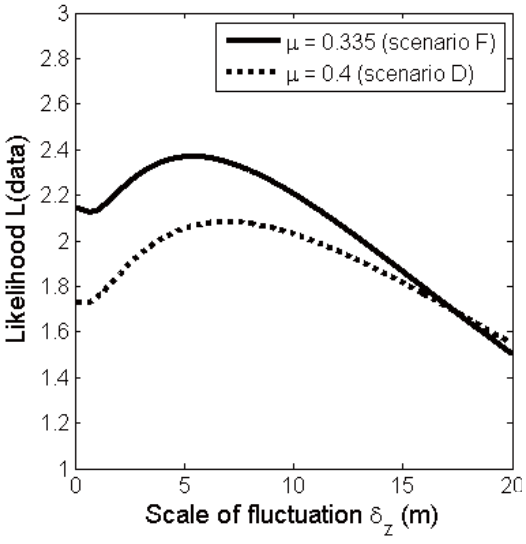

Fig. 4 The likelihoods of the two data points in Table 1 (versus δ_z) for the two scenarios

4. PROBABILITY MODEL FOR MINIMUM VALUE OF $t_f(z)$

Recall that $t_f(z)$ denotes $\tan[\phi(z)]$. The dip slope fails when $\tan[\phi(z)]$ < the limiting value of t_f for some $z \in [0, T]$. Let us denote the limiting value by $t_{f,L}$. In other words, the dip slope fails when $\min_{z \in [0,T]} t_f(z) < t_{f,L}$. If $t_f(z)$ is a stationary Gaussian random field, Ditlevsen (1966) derived the analytical expression for the probability that $\min_{z \in [0,T]} t_f(z) < t_{f,L}$. From now on, the minimum value $\min_{z \in [0,T]} t_f(z)$ will be denoted by $t_{f,\min}(T)$. Let us restrict ourselves to COV = 0.2. Based on the derivations in Ditlevsen (1966),

$$p_f = P\left[t_{f,\min}(T) < t_{f,L}\right] = 1 - \exp\left(-\frac{\varphi\left[(t_{f,L} - \mu)/(0.2\mu)\right]}{1 - \Phi\left[(t_{f,L} - \mu)/(0.2\mu)\right]} \cdot \gamma \cdot T\right) \cdot \left(1 - \Phi\left[(t_{f,L} - \mu)/(0.2\mu)\right]\right)^{1+G(T)} \quad (4)$$

where p_f denotes the failure probability; $\varphi(.)$ is the probability density function (PDF) of standard normal distribution; $\Phi(.)$ is the cumulative density function (CDF) of standard normal distribution; γ is a real number that is proportional to $1/\delta_z$; $G(T)$ is an increasing function of T that satisfies $G(0) = 0$. Ditlevsen (1966) did not derive the γ constant and the $G(T)$ function for the single exponential model in Eq. (2).

Note that the probability model in Eq. (4) is scalable: p_f depends on T/δ_z rather than on T alone. This scalability is illustrated in Table 4, where $p_f = P[t_{f,\min}(T) < t_{f,L}]$ is estimated using Monte Carlo simulations for some combinations of T and δ_z. 1000 samples of $t_f(z)$ profiles are first drawn using Monte Carlo simulation (assume scenario F). For each sampled $t_f(z)$ profile, the minimum value can be determined, hence 1000 samples of such minimum values are available. The probability $p_f = P[t_{f,\min}(T) < t_{f,L}]$ can then be estimated as the ratio that the 1000 sampled minimum values $< t_{f,L}$. Table 4 clearly shows that p_f only depends on T/δ_z. The minor difference in the p_f estimates under the same T/δ_z ratio is due to the variability of Monte Carlo simulation. Due to the scalability, Eq. (4) can be simplified into the following form:

$$p_f = 1-\exp\left(-\frac{\varphi\left[(t_{f,L}-\mu)/(0.2\mu)\right]}{1-\Phi\left[(t_{f,L}-\mu)/(0.2\mu)\right]}\cdot a\cdot\frac{T}{\delta_z}\right) \cdot\left(1-\Phi\left[(t_{f,L}-\mu)/(0.2\mu)\right]\right)^{1+b\cdot\frac{T}{\delta_z}} \quad (5)$$

where (a, b) are the two model parameters to be determined; note that $G(T)$ in Eq. (4) is taken to be $b \times T/\delta_z$. This is the simplest form of $G(T)$ that satisfies the requirement of being an increasing function, $G(0) = 0$, and being scalable.

There are two model parameters (a, b) in Eq. (5). To estimate (a, b), Monte Carlo simulation is used to simulate n samples of $t_f(z)$ profiles using the Fourier series method (Jha and Ching 2013). Each $t_f(z)$ profile is simulated with a chosen T and δ_z values. The minimum value of each $t_f(z)$ profile is determined and is taken to be a sample of $t_{f,\min}(T)$. The maximum likelihood method can be used to estimate (a, b) based on these n samples of $t_{f,\min}(T)$. Analysis results show that the optimal estimates for the two model parameters are $a = 2.00$ and $b = 1.87$ for the single exponential model in Eq. (2). With these two model parameters calibrated, the probability model in Eq. (5) performs fairly satisfactorily. Figure 5 shows the histograms of the 1000 simulated samples of $t_{f,\min}(T)$ for three occasions: (a) $T/\delta_z = 10$; (b) $T/\delta_z = 1$; and (c) $T/\delta_z = 0.1$. The mean value μ and COV are taken to be of scenario F, *i.e.*, $\mu = 0.335$ and COV = 0.2. The PDF for $t_{f,\min}(T)$ can be found by taking derivative of the right hand side CDF in Eq. (5) with respect to $t_{f,L}$. The PDFs are plotted as the solid lines in Fig. 5 – they are fairly close to the histograms of the 1000 simulated $t_{f,\min}(T)$ samples. Also plotted in the figure are the PDF of the point process $t_f(z)$ (dashed lines) – a normal distribution with mean $\mu = 0.335$ and COV = 0.2. It is clear that when T/δ_z is small, the PDF for $t_{f,\min}(T)$ is similar to the PDF of the point process $t_f(z)$. This is reasonable because when T/δ_z is small, there is nearly no fluctuation cycle in the [0, T] interval, *i.e.*, $t_f(z) \approx$ constant $\approx t_{f,\min}(T)$, hence the distribution of $t_{f,\min}(T)$ is similar to the distribution of $t_f(z)$. However, when T/δ_z is large, the PDF for $t_{f,\min}(T)$ shifts to the left and becomes substantially different from the PDF for the point process $t_f(z)$.

5. FAILURE PROBABILITY OF Freeway-3 DIP SLOPE

5.1 Limiting Value $t_{f,L}$

TGS (2011) conducted a series of three dimensional (3D) analyses using FLAC3D. The 5.5 m toe cut for the bridge launching pit in December 1997 is not introduced in such analyses because the purpose is to evaluate the stability status at the moment of landslide (the 5.5 m cut was backfilled after the construction in December 1997). Figure 6 shows the relationship between the displacment at a reference point on slope face and the assumed friction angle ϕ on the failure surface. This relationship is plotted for various remaining anchor force (RAF), in term of a fraction to its design value (60 tons). If the limiting displacement d_L is 10 cm (displacement > d_L denotes failure), the slope fails when $\phi < 12.4°$ when RAF = 100% of its design value, *i.e.*, $t_{f,L} = \tan(12.4°) = 0.220$. If $d_L = 100$ cm, the slope fails when $\phi < 11.8°$ (extrapolated) when RAF = 100% of its design value, *i.e.*, $t_{f,L} = \tan(11.8°) = 0.209$. Table 5 lists the values of $t_{f,L}$ for various RAFs.

The p_f of the Freeway-3 dip slope with a prescribed RAF can be calculated based on the $t_{f,L}$ value found from Table 5. Let us take scenario F as an example ($\mu = 0.335$, COV = 0.2, $\delta_z = 5.5$ m).

Table 4 The p_f estimates made by Monte Carlo simulations for some combinations of T and δ_z

T (m)	δ_z (m)	T/δ_z	$p_f = P[t_{f,\min}(T) < t_{f,L}]$	
			$t_{f,L} = 0.3$	$t_{f,L} = 0.2$
100	10	10	1.00	0.73
10	1		1.00	0.74
1	0.1		1.00	0.76
100	100	1	0.79	0.17
10	10		0.80	0.15
1	1		0.80	0.16
100	1000	0.1	0.42	0.034
10	100		0.45	0.037
1	10		0.44	0.048

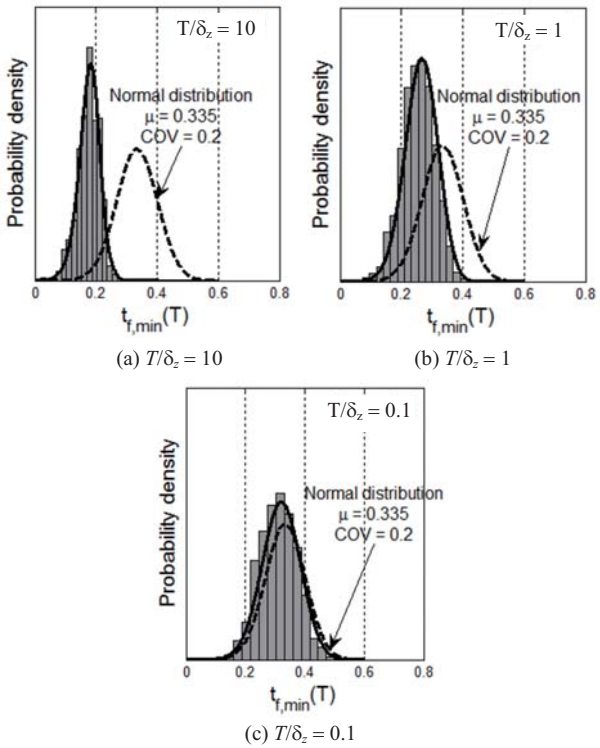

(a) $T/\delta_z = 10$ (b) $T/\delta_z = 1$

(c) $T/\delta_z = 0.1$

Fig. 5 The histograms of the 1000 simulated samples of $t_{f,\min}(T)$ for three occasions

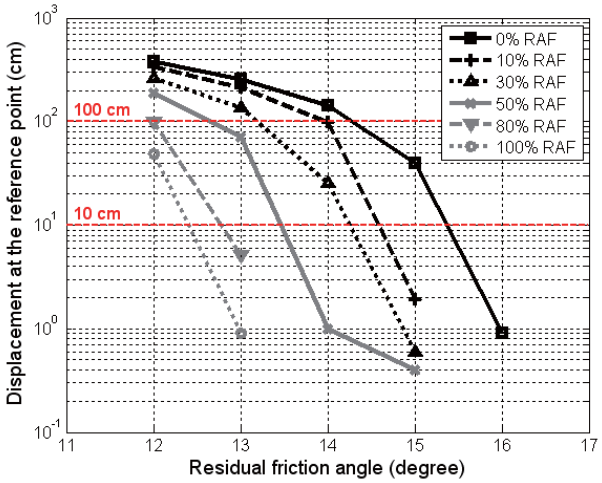

Fig. 6 The relationship between the displacment at a reference point and residual friction angle [based on Fig. 6 ~ 64 in TGS (2011)]

Table 5 The values of $t_{f,L}$ for various remaining anchor forces (RAFs)

% RAF/ (design force 60 tons)		100%	80%	50%	30%	10%	0%
Limiting value of ϕ	d_L = 10 cm	12.4°	12.8°	13.5°	14.3°	14.6°	15.3°
	d_L = 100 cm	11.8°*	12.0°	12.7°	13.2°	14.0°	14.3°
$t_{f,L}$	d_L = 10 cm	0.220	0.227	0.240	0.255	0.261	0.274
	d_L = 100 cm	0.209	0.213	0.225	0.235	0.249	0.255

* Extrapolated values

Recall that the thickness of the critical layer is about 4 m (T = 4 m). Consider the case where RAF = 0% and the limiting displacement d_L = 10 cm. For this case, $t_{f,L}$ = 0.274 can be checked from Table 5, and δ_z = 5.5 m can be checked from Table 3. The p_f is therefore

$$p_f = 1-\exp\left(-\frac{\varphi\left[(0.274-0.335)/(0.2\cdot 0.335)\right]}{1-\Phi\left[(0.274-0.335)/(0.2\cdot 0.335)\right]}\cdot 2.0\cdot\frac{4}{5.5}\right)$$
$$\cdot\left(1-\Phi\left[(0.274-0.335)/(0.2\cdot 0.335)\right]\right)^{1+1.87\cdot\frac{4}{5.5}} = 0.61 \quad (6)$$

This p_f estimate of 0.61 is surprisingly high. The left plot in Fig. 7 shows the histogram of $t_{f,\min}(T)$ under scenario F (μ = 0.335, COV = 0.2, and δ_z = 5.5 m) – the chance for $t_{f,\min}(T) < t_{f,L}$ = 0.274 is indeed fairly high. The high p_f is confirmed in Fig. 8 that shows five random samples of $t_f(z)$ profiles under scenario F – three of them have $t_{f,\min}(T)$ < 0.274 (failure). If the spatial variability of $t_f(z)$ is not considered, *i.e.*, δ_z is infinite, p_f can be determined:

$$p_f = 1-\exp\left(-\frac{\varphi\left[(0.274-0.335)/(0.2\cdot 0.335)\right]}{1-\Phi\left[(0.274-0.335)/(0.2\cdot 0.335)\right]}\cdot 2.0\cdot\frac{4}{\infty}\right)$$
$$\cdot\left(1-\Phi\left[(0.274-0.335)/(0.2\cdot 0.335)\right]\right)^{1+1.87\cdot\frac{4}{\infty}}$$
$$= \Phi\left[(0.274-0.335)/(0.2\cdot 0.335)\right] = 0.18 \quad (7)$$

In this case, the $t_f(z)$ profile is a constant function, so $t_f(z) = t_{f,\min}(T)$ = constant. The right plot in Fig. 7 shows the histogram of $t_{f,\min}(T)$ with $\delta_z = \infty$ – the chance for $t_{f,\min}(T)$ < 0.274 is indeed smaller. This demonstrates the importance of considering spatial variability. The p_f will be seriously underestimated if the spatial variability in $t_f(z)$ is ignored.

Figure 9 shows how p_f changes with RAF for scenarios D and F. The p_f is plotted as a range: Upper bound for d_L = 10 cm and lower bound for d_L = 100 cm. It is correct that p_f decreases with increasing RAF. Scenario F has larger p_f, as μ = 0.335 is smaller than that for scenario D. If the spatial variability of $t_f(z)$ is not considered ($\delta_z = \infty$), Figure 10 shows how p_f changes with RAF for scenarios D and F. Again, it is clear that p_f will be seriously underestimated if the spatial variability in $t_f(z)$ is ignored.

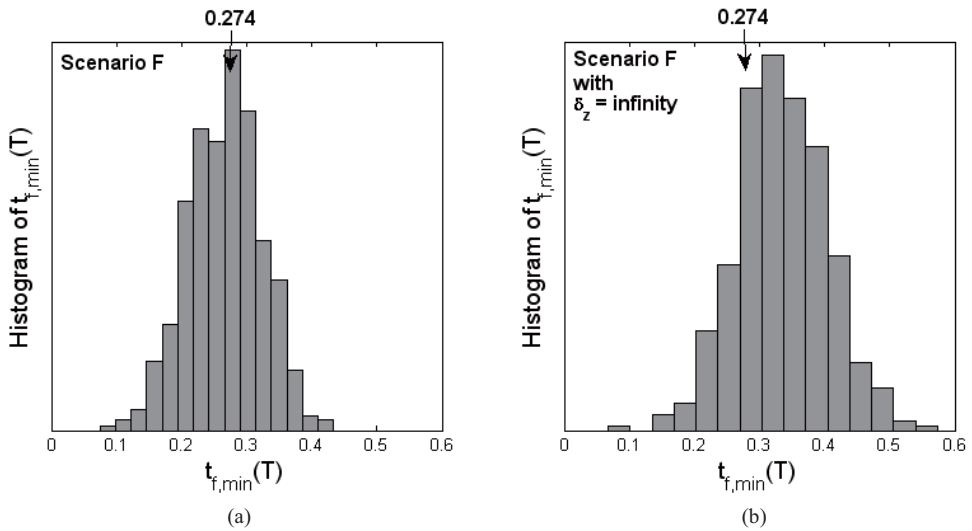

Fig. 7 (a) Histogram of $t_{f,\min}(T)$ for scenario F; (b) histogram of $t_{f,\min}(T)$ for scenario F with $\delta_z = \infty$ (no spatial variability)

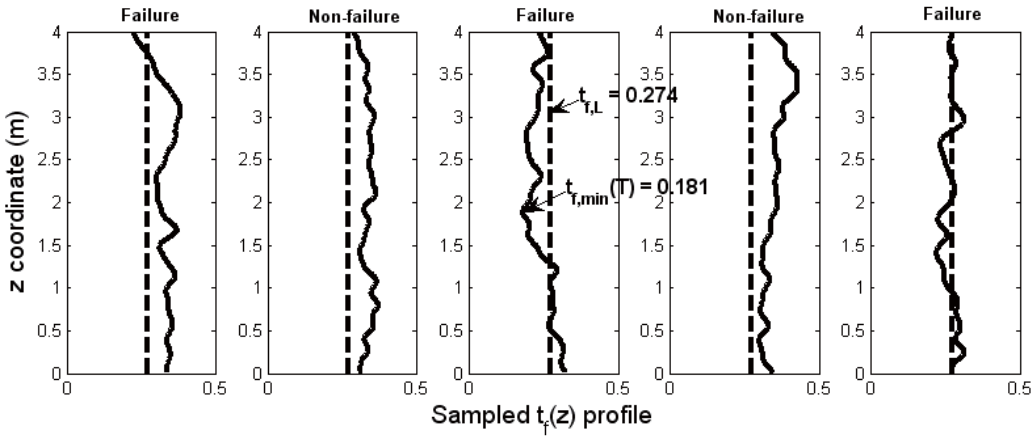

Fig. 8 Five samples of $t_f(z)$ profiles under scenario *F* ($\mu = 0.335$, COV = 0.2, $\delta_z = 5.5$ m)

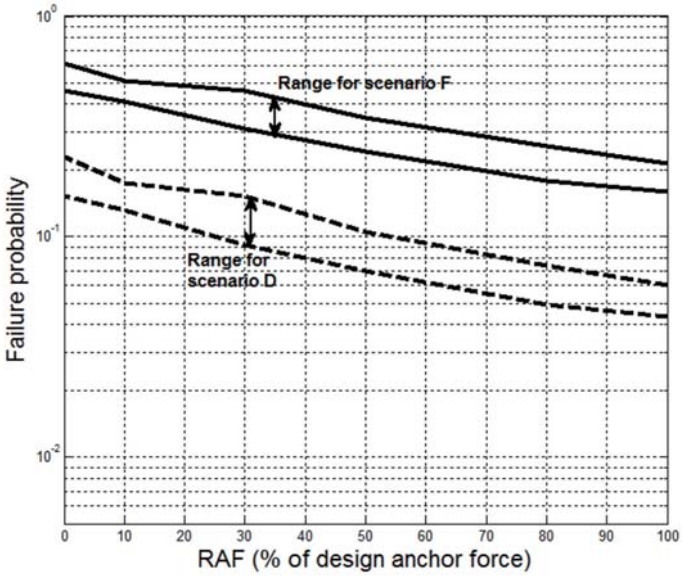

Fig. 9 The ranges of p_f for scenarios *D* and *F*

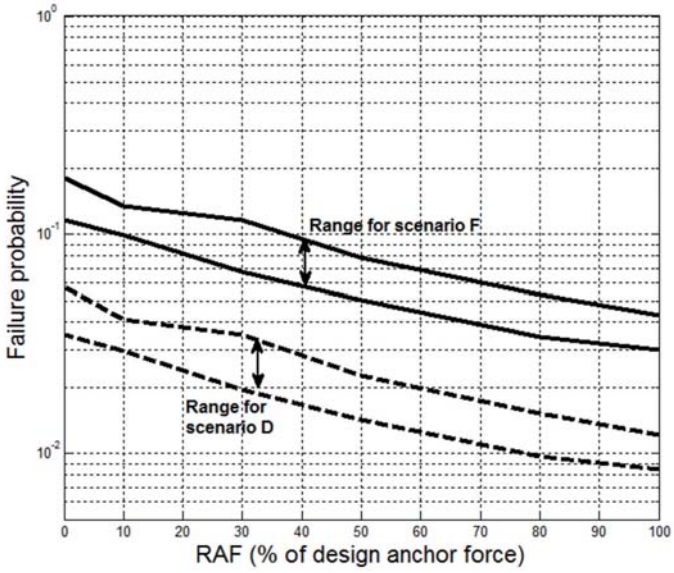

Fig. 10 The ranges of p_f for scenarios *D* and *F* with $\delta_z = \infty$ (no spatial variability)

5.2 Appropriateness of the Original Design for the Freeway-3 Dip Slope

5.2.1 Appropriateness under Scenario D without Considering Spatial Variability

As mentioned earlier, during the design stage in 1995 the nominal value of ϕ is chosen to be 20° and c is chosen to be 9.8 kN/m^2. This represents the information status at that time and is close to scenario *D* ($\mu = 0.4$). At the design stage, spatial variability was not considered. The p_f value with 100% RAF but without considering spatial variability ($\delta_z = \infty$) ranges from 0.0085 ~ 0.012 (see Fig.10).

Whitman (1984) developed the risk chart shown in Fig. 11. Note that the vertical axis is the annual p_f. There are two important risk boundaries:

$$p_f = 0.063 \cdot N^{-0.575} = \text{boundary for "marginally accepted"}$$
$$p_f = 0.025 \cdot N^{-0.7} = \text{boundary for "accepted"} \quad (8)$$

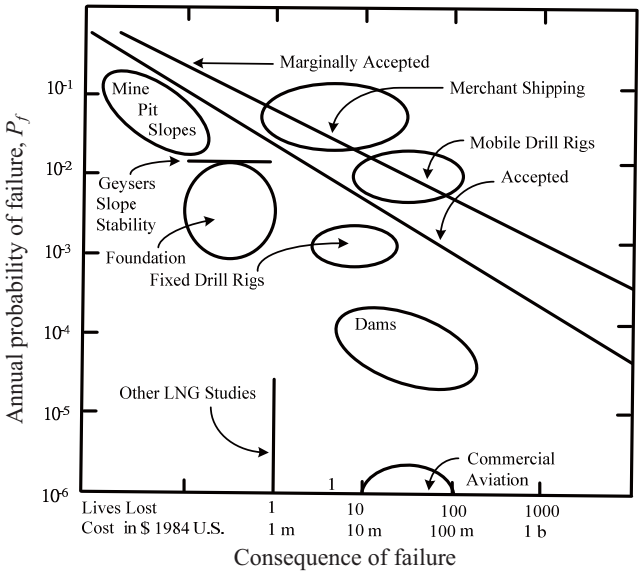

Fig. 11 The risk chart proposed by Whitman (1984) for built engineering systems (redrawn)

where N denotes the number of fatalities. The Freeway-3 failure case caused four fatalities (N = 4). With N = 4, the above two boundaries correspond to p_f = 0.095 and 0.028. Another useful boundary was mentioned in U.S. Army Corps of Engineers (1997):

$$p_f = 0.16 = \text{boundary for "hazardous"} \tag{9}$$

As a result, the following risk level is adopted for the Freeway-3 case:

$$\text{Risk level for the F-3 case} = \begin{cases} \text{Accepted} & p_f \le 0.028 \\ \text{Intermediate} & 0.028 < p_f \le 0.095 \\ \text{Unaccepted} & 0.095 < p_f \le 0.16 \\ \text{Hazardous} & p_f > 0.16 \end{cases} \tag{10}$$

According to Eq. (10), the previous p_f range of 0.0085 ~ 0.012 is classified as "accepted". In other words, the design under scenario D without considering spatial variability is deemed acceptable when RAF = 100%. Note that this association of the p_f range of 0.0085 ~ 0.012 to the class "accepted" is based on the assumption that the annual p_f in Fig. 11 (vertical axis) can be compared with the p_f value computed by (5). The risk levels when RAF = 50% and 0% under scenario D without considering spatial variability are also listed in the left half of Table 6. The risk level is still acceptable for RAF = 50% and becomes intermediate for RAF = 0%. In overall, the design for the Freeway-3 dip slope seems satisfactory under scenario D without considering spatial variability.

5.2.2 Appropriateness under Scenario *D* Considering Spatial Variability

The right half of Table 6 shows the risk levels under scenario D when spatial variability is considered (δ_z is taken to be 7.0 m, as seen in Table 3 for scenario D). The risk levels greatly worsen when spatial variability is considered. The risk level is now intermediate when RAF = 100%, unacceptable when RAF = 50%, and hazardous when RAF = 0%. If spatial variability, a realistic phenomenon in soils and rocks, of the critical layer were considered in the design stage in 1995, a more conservative design could have been mandated. However, the above spatial variability analysis requires the knowledge for the location of the critical layer. The dilemma is that it is challenging to identify its location before the failure actually occurred.

5.2.3 Appropriateness under Scenario *F*

Table 7 shows the risk levels under scenario F – the left half of the table lists the results without considering spatial variability, and the right half lists the results considering spatial variability. One important conclusion is that the risk levels under scenario F further worsen, compared to scenario D. In particular, the risk levels for the cases considering spatial variability are all hazardous.

In summary, the design of the Freeway-3 dip slope made in 1995 seems satisfactory (a) if spatial variability is not considered and (b) if new information such as those obtained during the 2010 forensic investigation is not known. However, if one of the above two aspects [(a) or (b)] were considered, a more conservative

Table 6 Risk levels under scenario D

	Without considering spatial variability (μ = 0.4, COV = 0.2, $\delta_z = \infty$)			Considering spatial variability (μ = 0.4, COV = 0.2, δ_z = 7.0 m)		
% RAF	100%	50%	0%	100%	50%	0%
p_f	0.0085 ~ 0.012	0.014 ~ 0.023	0.035 ~ 0.058	0.043 ~ 0.060	0.070 ~ 0.11	0.15 ~ 0.23
Risk level	Accepted	Accepted	Intermediate	Intermediate	Unaccepted	Hazardous *

* Mostly hazardous

Table 7 Risk levels under scenario F

	Without considering spatial variability (μ = 0.335, COV = 0.2, $\delta_z = \infty$)			Considering spatial variability (μ = 0.335, COV = 0.2, δ_z = 5.5 m)		
% RAF	100%	50%	0%	100%	50%	0%
p_f	0.030 ~ 0.043	0.050 ~ 0.078	0.12 ~ 0.18	0.16 ~ 0.22	0.24 ~ 0.34	0.46 ~ 0.61
Risk level	Intermediate	Intermediate	Unaccepted*	Hazardous	Hazardous	Hazardous

* Mostly unaccepted

design could have been mandated. In fact, considering spatial variability alone could have mandated a more conservative design. If both aspects [(a) and (b)] were considered, the original Freeway-3 design is found to be hazardous for all RAFs (even with 100% RAF!).

5.3 Sudden Increase in Anchor Force during Construction in December 1997

As mentioned earlier, during the construction stage in December 1997, the anchor loads suddenly increased from around 70 tons to 76 ~ 87 tons. This sudden increase in the anchor loads cannot be explained as the consequence of the anchor corrosion and bedding plane degradation, as both require a long period of time. It is likely that the dip slope would have failed at that moment if the anchors were not there (RAF = 0%). Table 7 shows the risk levels when RAF = 0%. These risk levels are based on FLAC3D analyses in Fig. 6, for which the 5.5 m toe cut for bridge launching was backfilled. This deviates from the real situation in December 1997 – the 5.5 m cut was still there. Hence, it is expected that the actual risk levels in December 1997 are worse than those in Table 7. The left half of the table lists the results when spatial variability is not considered, and the right half lists the results when spatial variability is considered. Without considering spatial variability, the risk levels for scenarios *D* and *F* are, respectively, intermediate and unaccepted. Both risk levels turn into hazardous if spatial variability is considered, *i.e.*, when spatial variability is considered, the Freeway-3 dip slope is more likely to have failed when there were no anchors. Spatial variability seems to be able to explain the sudden increase in the anchor loads.

6. RISK-BASED DESIGN FOR A FUTURE CASE SIMILAR TO Freeway-3 DIP SLOPE

The following steps are suggested for the risk calculation and design of a future case that is similar to the Freeway-3 case. These steps take spatial variability of shear strength into account, but detailed analysis for spatial variability is not needed, as the analytical solution for p_f under spatial variability has been calibrated.

1. Identify the critical layer. In general, this is fairly challenging. The following steps cannot proceed without such identification. Once the critical layer is identified, find its thickness (T), location, inclination angle, *etc*. Estimate the possible number (N) of fatalities if this slope fails. Such estimation can be based on local experiences or based on literature such as Guzzetti (2000) and Petley *et al*. (2005). A range of N can be given if the uncertainty is large. In this case, the resulting risk level will be also a range.
2. Obtain n rock samples from the critical layer using boreholes, preferably with more than three samples ($n > 3$). Record the z-coordinates (z_1, z_2, …, z_n) in the N-direction for these samples. Try to make the positions (z_1, z_2, …, z_n) as distinct as possible. Let the residual friction angles of these samples be (ϕ_1, ϕ_2, …, ϕ_n). The mean value of $t_f = \tan(\phi)$ can be estimated as $\mu = [\tan(\phi_1) + \tan(\phi_2) + \ldots + \tan(\phi_n)]/n$. The COV of t_f can be taken as 0.2 – this number is especially suitable for SS/SH and SH in northern Taiwan.
3. The SOF in the N-direction (δ_z) of the critical layer can be estimated by maximizing the following likelihood function:

$$L(\text{data}) = \frac{1}{2\pi}\frac{1}{\sqrt{|\Sigma|}}\exp\left(-0.5\begin{bmatrix}\tan(\phi_1)-\mu\\ \tan(\phi_2)-\mu\\ \vdots\\ \tan(\phi_n)-\mu\end{bmatrix}^T \Sigma^{-1}\begin{bmatrix}\tan(\phi_1)-\mu\\ \tan(\phi_2)-\mu\\ \vdots\\ \tan(\phi_n)-\mu\end{bmatrix}\right)$$

$$\Sigma = (0.2\mu)^2\begin{bmatrix}1 & \exp\left(-2|z_1-z_2|/\delta_z\right) & \cdots & \exp\left(-2|z_1-z_n|/\delta_z\right)\\ & 1 & & \exp\left(-2|z_2-z_n|/\delta_z\right)\\ & & \ddots & \vdots\\ \text{symmetry} & & & 1\end{bmatrix} \tag{11}$$

where $\mu = [\tan(\phi_1) + \tan(\phi_2) + \ldots + \tan(\phi_n)]/n$ is a known constant.

4. Run a series of deterministic back-calculation slope analyses similar to those in Fig. 6. Identify the limiting value $t_{f,L}$ based on the analysis results.
5. Given the limiting value $t_{f,L}$, the failure probability can be calculated by

$$p_f = 1-\exp\left(-\frac{\varphi\left[(t_{f,L}-\mu)/(0.2\mu)\right]}{1-\Phi\left[(t_{f,L}-\mu)/(0.2\mu)\right]}\cdot 2.0\cdot\frac{T}{\delta_z}\right)\cdot\left(1-\Phi\left[(t_{f,L}-\mu)/(0.2\mu)\right]\right)^{1+1.87\cdot\frac{T}{\delta_z}} \tag{12}$$

where $\varphi(x)$ and $\Phi(x)$ can be evaluated by excel function NORMDIST(x, 0, 1, index) [index = 0 for $\varphi(x)$ and index = 1 for $\Phi(x)$].

6. Find the risk level of this future case by the following criterion:

$$\text{Risk level} = \begin{cases}\text{Accepted} & p_f \le 0.025\cdot N^{-0.7}\\ \text{Intermediate} & 0.025\cdot N^{-0.7} < p_f \le 0.063\cdot N^{-0.575}\\ \text{Unaccepted} & 0.063\cdot N^{-0.575} < p_f \le 0.16\\ \text{Hazardous} & p_f > 0.16\end{cases} \tag{13}$$

7. Iterate the design configuration (*e.g.*, anchor force) until the risk level is satisfactory, either being accepted or intermediate, depending on the problem at hand.

7. CONCLUSIONS

This study re-analyzes the Freeway-3 (F-3) dip slope failure case, emphasizing the impact of spatial variability of the shear strength inside the slope. It is shown that under the information available at the time of the design stage (around 1995), the original Freeway-3 design had a fairly acceptable risk level, even when the anchor force reduced to zero. However, this scenario is based on analyses without considering spatial variability in shear strength. Detailed analysis shows that if spatial variability is properly modeled and considered, the risk level dramatically worsens to "intermediate" when the anchor has its full design force, and to "hazardous" when the anchor force is zero. This implies that the consideration of spatial variability is essential for the Freeway-3 case.

Without considering spatial variability, the risk level with zero anchor force is not particularly high (intermediate), *i.e.*, the slope may stand on its own. This contradicts with the observed sudden increase in the anchor load during the construction stage in December 1997. Nonetheless, when spatial variability is considered, the risk level with zero anchor force jumps to "hazardous", *i.e.*, the slope may not stand on its own. This is consistent to the observed sudden increase in the anchor load. Spatial variability seems to be able to explain the sudden increase in the anchor loads for the Freeway-3 case. However, this sudden increase in the anchor loads cannot be easily explained by the anchor corrosion and rock degradation.

The new shear strength data obtained during the forensic investigation in 2010 provides extra evidence why the Freeway-3 dip slope failed. The calculated risk levels based on the 2010 data significantly worsen, compared to those based on the 1995 data. This implies that the extent and quality of the site investigation in the design stage in 1995 may not be sufficient.

Analysis results also show that if the 2010 data is adopted and if spatial variability is properly considered during the design stage, the risk level becomes "hazardous" even when the anchors have full design loads.

Simple risk-based design steps are proposed near the end of this paper. These steps require carefully planned site investigation, a rough estimate of the consequence (number of fatalities), solving a one-dimensional optimization problem to estimate the scale of fluctuation, and a set of deterministic slope analyses. Detailed analysis for spatial variability is not needed, as the analytical solution for the failure probability under spatial variability has been calibrated. The outcome is the risk level of the slope of interest. One needs to iterate the design configuration to reach a satisfactory design.

The analysis presented in the paper is based on residual shear strengths. The possible corrosion of the anchors and the possible degradation of residual strengths due to disturbances and wetting are not considered. If these factors are considered, the long term risk level will further worsen. More importantly, the analyses in this study are based on a premise – the critical layer is identified beforehand. The identification of the critical layer itself is a challenging task. The purpose of this study is not to address how to identify such a critical layer beforehand. Rather, its purpose is to conduct a forensic analysis about the impact of spatial variability in the critical layer and to provide plausible explanation to some observed phenomena, given that the critical layer has been identified.

ACKNOWLEDGEMENTS

This study was under the sponsorship of the National Science Council (NSC) of Republic of China, under the project NSC100-2628-E-002-040-MY3. The first author would like to acknowledge such a gracious support from NSC.

REFERENCES

Ching, J., Yang, Z. Y., Shiau, J. Q., and Chen, C. J. (2012). "Estimation of rock pressure during an excavation/cut in sedimentary rocks with inclined bedding planes." *Structural Safety*, **41**, 11–19.

Ditlevsen, O. (1966). "Extremes of realizations of continuous time stationary stochastic processes on closed intervals." *Journal of Mathematical Analysis and Applications*, **14**, 463–474.

Guzzetti, F. (2000). "Landslide fatalities and the evaluation of landslide risk in Italy." *Engineering Geology*, **58**, 89–107.

Jha, S. K. and Ching, J. (2013). "Simulating spatial averages of stationary random field using Fourier series method." *Journal of Engineering Mechanics*, ASCE, **139**(5), 594–605.

Petley, D. N., Dunning, S. A., and Rosser, N. J. (2005). "The analysis of global landslide risk through the creation of a database of worldwide landslide fatalities." in Hungr, O., *et al.* (Eds.), *Landslide Risk Management*, Amsterdam, A.A. Balkema, 367–374.

Phoon, K. K. (1995). *Reliability-Based Design of Foundations for Transmission Line Structures*. Ph.D. Dissertation, Cornell University, Ithaca, NY.

Phoon, K. K., Quek, S. T., and An, P. (2003). "Identification of statistically homogeneous soil layers using modified Bartlett statistics." *Journal of Geotechnical and Geoenvironmental Engineering*, ASCE, **129**(7), 649–659.

TGS (2011) *Forensic Study on the Dip Slope Failure of Freeway No.3 at Chainage 3.1K*, Investigation Report, Taiwan Geotechnical Society, Taipei (in Chinese).

U.S. Army Corps of Engineers (1997). "Engineering and design, introduction to probability and reliability methods for use in geotechnical engineering." *Engineering Technical Letter No. 1110-2-547*, Dept of the Army, Washington, D.C.

Vanmarcke, E. H. (1977). "Probabilistic modeling of soil profiles." *Journal of Geotechnical Engineering Division*, ASCE, **103**(11), 1227–1246.

Wang, L., Hwang, J. H., Luo, Z., Juang, C. H., and Xiao, J. (2013). "Probabilistic back analysis of slope failure – a case study in Taiwan." *Computers and Geotechnics*, **51**, 12–23.

Whitman, R. V. (1984). "Evaluating calculated risk in geotechnical engineering." *Journal of Geotechnical Engineering*, ASCE**,** **110**(2), 143–188.